Synthesis, Crystal Structure and Fluorescent Properties of New Layered Thiophosphate $Cs_2Ga_3PS_8$①

CHEN Wen-Fa[a, b] LIU Bin-Wen[a]
JIANG Xiao-Ming[a②] GUO Guo-Cong[a②]
[a] (*State Key Laboratory of Structural Chemistry, Fujian Institute of Research on the Structure of Matter, Chinese Academy of Sciences, Fuzhou* 350002, *China*)
[b] (*University of Chinese Academy of Sciences, Beijing* 100190, *China*)

ABSTRACT A new quaternary metal thiophosphate, $Cs_2Ga_3PS_8$, in triclinic $P\bar{1}$ space group has been successfully synthesized by a reactive-flux method. Its structural framework is derived from well-known $AM^{III}M^{IV}Q_4$ (A = alkali metal; M^{III} = Al, Ga, In; M^{IV} = Si, Ge, Sn; Q = S, Se) system and composed of two-dimensional $^2_\infty[Ga_3PS_8]^{2-}$ layers separated by Cs^+. The compound exhibits a wide band gap of 3.08 eV and congruent-melting behavior with melt point of 645 ℃. Interestingly, $Cs_2Ga_3PS_8$ exhibits a broad photoluminescent emission band at 420 nm upon excitation at 295 nm. Moreover, electronic structure calculations indicate that $Cs_2Ga_3PS_8$ is a direct band gap compound and its luminescent process can be mainly ascribed to electron transfer from the S-3*p* and Ga-4*p* states to S-3*p* and P-3*p*.

Keywords: chalcogenide, thiophosphate, crystal structure, solid-state phase, synthesis;
DOI: 10.14102/j.cnki.0254-5861.2011-3135

1 INTRODUCTION

In the past decades, many achievements have been made in exploring functional materials in chalcogenides, which can be used as nonlinear optics, electro optics, superionic conductors, and pyroelectrics[1-10]. As an important subgroup of chalcogenide, thiophosphates exhibit rich structural diversity as well as unique physical properties, and have received broad attention[11-15]. Thiophosphates are typically composed of tetrahedral $[PQ_4]^{3-}$ (Q = S, Se, Te) and ethane-like $[P_2Q_6]^{4-}$ units, the combination of which could further generate more complex building blocks such as $[P_2Se_6]^{4-}$[16], $[P_2Se_9]^{4-}$[17], and infinite chains like $[P_2Se_6]^{2-}$[18], $[PSe_6]^{-}$[19], $[P_5Se_{10}]^{5-}$[20]. Moreover, discrete $[P_xQ_y]^{n-}$ fragments can be assembled with other metals to form a variety of extended frameworks with fascinating properties. For example, $A_4GeP_4Se_{12}$ (A = K, Rb, Cs) are excellent IR NLO materials exhibiting large second-harmonic-generation effect which is ~30 times that of bench $AgGaSe_2$ at 730 nm[21]. $AZrPS_6$ (A = K, Rb, Cs) are unique examples of stable inorganic semiconductors with band gap emission very attractive for technological applications[22]. $Rb_4Sn_5P_4Se_{10}$ is a semimetallic selenophosphate and displays high conductivity of 51 S/cm at 300 K[23]. $Li_{10}SnP_2S_{12}$ is an affordable lithium superionic conductor with very high values of 7 mS/cm for the grain conductivity[24]. Although many thiophosphates have been found, investigations on thiophosphates containing Ga are rare. During our attempts to explore A–Ga–P–Q system, a new phase, $Cs_2Ga_3PS_8$ (**1**), has been synthesized. Herein, the syntheses, structures, and thermal and optical properties of **1** are presented. Interestingly, the compound exhibits a broad photoluminescent emission band at 420 nm. To gain further insights on its luminescent properties, the calculations of electronic band structure and density of states were performed.

2 EXPERIMENTAL

2. 1 Syntheses

The following reagents were used as obtained: Ba metal (99.9%), Ga metal (99.99%), P powder (99.99%), S powder (99.99%), and CsCl powder (99.99%). All operations were handled under an Ar atmosphere in a glove box. The title

Received 5 February 2021; accepted 2 April 2021 (**ICSD 416574**)
① This work was supported by the NSF of China (21827813, 21921001, 22075283), Scientific Research Fund of Natural Science Foundation of Fujian Province (2020J01115) and the Youth Innovation Promotion Association of CAS (No. 20200303)
② Corresponding authors. E-mails: gcguo@fjirsm.ac.cn and xmjiang@fjirsm.ac.cn

compound was synthesized by the stoichiometric mixture of Ba, Ga, P, S, and CsCl with total mass of 500 mg in a molar ratio of 1:3:1:8:2. The mixture was loaded into quartz tubes and then flame-sealed. The tubes were placed into a computer-controlled furnace, heated to 750 ℃ over 24 hours, subsequently dwelled for 4 days, and finally cooled down to room temperature at 3 ℃/hour. After the products were washed with deionized water and dried with methanol, lamellar colorless single crystals of **1** were observed, and the samples for further property measurements were obtained by hand picking under a microscope.

2. 2 Single-crystal X-ray diffraction

Single-crystal X-ray diffraction measurement was performed on a Rigaku Pilatus CCD diffractometer using a graphite-monochromated Mo-*Kα* radiation (λ = 0.71073 Å) at 293 K. The intensity dataset of the title compound was collected using an ω-scan technique and reduced using the CrysAlisPro[25]. The structure was solved by direct methods and refined with full-matrix least-squares methods on F^2 with anisotropic thermal parameters for all atoms[26].

2. 3 X-ray powder diffraction

Powder X-ray diffraction (XRD) data were recorded on an automated Rigaku MiniFlex II X-ray diffractometer equipped with a diffracted monochromator set for Cu-*Kα* radiation (λ = 1.54057 Å), operating at 30 kV and 40 mA. The observed powder pattern of the title compound was well-suited to the simulated one (Fig. S1b).

2. 4 Elemental analysis

Selected crystals were fixed on the sample platform and analyzed by energy dispersive analyses X-ray spectroscopy (EDX) by using an EDX-equipped Hitachi S-3500 SEM spectrometer. Energy dispersive spectroscopy (EDS) analysis of the crystals of the title compound confirmed the presence of Cs/Ga/P/S with a molar ratio of 2.0/2.9/1.1/7.8, which is close to that determined from the single-crystal X-ray diffraction analysis (Fig. S1a).

2. 5 UV-Vis diffuse reflectance spectroscopy

Optical diffuse reflectance measurement was made to measure the band gap of the title compound by Perkin-Elmer Lambda 900 UV-Vis spectrophotometer accompanied with an integrating sphere attachment, with $BaSO_4$ used as a reference. Absorption spectrum was calculated from the reflection spectrum using the Kubelka-Munk formula: $\alpha/S = (1 - R)^2/2R$[27], in which α is the absorption coefficient, S the scattering coefficient, and R the reflectance.

2. 6 Photoluminescence

The photoluminescence (PL) measurement of **1** was conducted on a single-grating Edinburgh EI920 fluorescence spectrometer equipped with a 450 W Xe lamp and a PMT detector.

2. 7 Thermal analysis

Thermal properties of the title compound were measured by differential scanning calorimetry (DSC) with a TGA/DSC Mettler Toledo thermal analyzer. Polycrystalline sample (approximately 10 mg) was put into a quartz tube, then evacuated to $\sim 10^{-4}$ Torr and sealed. Finally, the tube experienced a heating/cooling cycle at a rate of 10 ℃/min.

2. 8 Electronic structure calculation

The electronic band structure and density of state (DOS) of **1** were calculated by the CASTEP code[28] on the basis of density functional theory (DFT)[29], using a plane-wave expansion of the wave functions and an ultra-soft pseudo potential. The orbital electrons of Cs $5s^25p^66s^2$, Ga $3d^{10}4s^24p^1$ and S $3s^23p^4$ were treated as valence electrons. A plane-wave cutoff energy was set to be 295 eV with a grid of Monkhorst-Pack k-points of 4×4×2.

3 DISCUSSION

3. 1 Structure description

Compound **1** crystallizes in monoclinic space group of $P\bar{1}$ (No. 2) with a = 7.22730(10), b = 7.64670(10), c = 14.2671(3) Å, α = 91.005(2), β = 91.146(2), γ = 106.016(2)°, V = 757.50(2) Å^3 and Z = 2. The asymmetric unit is depicted in Fig. 1a. There are two crystallographically independent Cs atoms, two Ga atoms, eight S atoms, and two mixed positions with equal occupancy of Ga and P. The title compound exhibits a two-dimensional layer structure (Fig. 2a). All Ga and P atoms are tetrahedrally coordinated by S atoms to form GaS_4 and $(Ga/P)S_4$ tetrahedra. GaS_4 tetrahedra share two corners with each other to form 13 tetrahedra chains extending along the a direction, which are further bridged by $(Ga/P)S_4$ tetrahedra dimers alternately, forming a $[Ga_3PS_8]^{2-}$ layer in the ac plane (Fig. 2b). The $(Ga/P)S_4$ tetrahedra dimers are constructed by two edge-shared $(Ga/P)S_4$ tetrahedra. The counter Cs^+ are embedded between $[Ga_3PS_8]^{2-}$ layers.

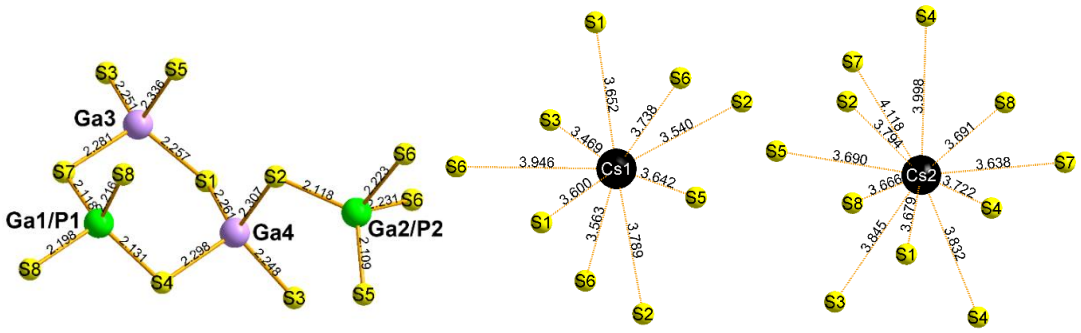

(a) **(b)**

Fig. 1. Coordination environments of Ga and P atoms (a), and ionic interactions around Cs atoms (b) in the asymmetric unit of 1

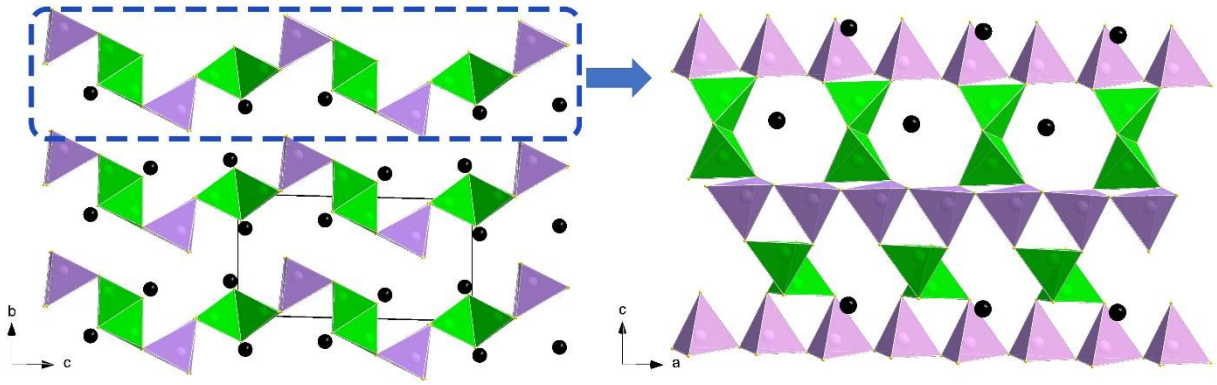

(a) **(b)**

Fig. 2. (a) Crystal structure of 1 viewed along the *a* axis. (b) A $[Ga_3PS_8]^{2-}$ layer.
Green and purple tetrahedra represent (Ga/P)S_4 and GaS_4 units, respectively. Black balls in (a) are Cs atoms

Compound **1** belongs to $Cs_2M_3^{III}M^{V}Q_8$ (Q = S, Se, Te) family (type-I)[30], which can be derived from $AM^{III}M^{IV}Q_4$ family (type-II)[31, 32] by replacing all M^{IV} atoms with equal amounts of M^{III} and M^{V} atoms. The modification of $AM^{III}M^{IV}Q_4$ family can also lead to $A_2M^{II}M^{IV}{}_3Q_8$ (Q = S, Se, Te) family (type-III) via the substitution of two M^{III} atoms by one M^{II} and one M^{IV} atoms[33-35]. The structures of type-I, II and III compounds are similar, but they exhibit different structure disorders of tetrahedrally coordinated centers. In type-II compounds, the trivalent and tetravalent metal ions are disordered over all tetrahedral sites. Type-III family of compounds is completely ordered, whereas in the type-I compounds, all M^{V} and partial M^{III} positions are disordered. The flexible substitution behavior of $AM^{III}M^{IV}Q_4$ family makes it a good platform for exploring new materials with rich structure features and physical properties[31, 32].

As listed in Table S2, Ga–S distances of fully occupied GaS_4 tetrahedra in **1** are in the range of 2.2484～2.3361 Å, which are close to those in β-$LaGaS_3$ (2.194～2.325 Å)[36] and $SnGa_4S_7$ (2.214～2.337 Å)[37]. In (Ga/P)S_4 tetrahedra, the Ga/P–S distances range from 2.1087 to 2.2309 Å, which are between the typical P–S and Ga–S bond lengths. Two crystallographically independent Cs atoms are surrounded by nine and eleven S atoms, respectively, with ionic interactions. The Cs–S distances in the range of 3.469～4.118 Å (Fig. 1b) are consistent with those in $Cs[Lu_7S_{11}]$[38].

3. 2 Experimental band gap and photoluminescent spectra

The UV-Visible-NIR diffuse reflectance spectrum of **1** exhibits obvious absorption edge and the band gap is estimated to 3.05 eV (Fig. 3a), which is consistent with its colorless feature. The band gap of **1** is comparable to those of some other thiophosphates, such as $KAg_2[PS_4]$ (3.02 eV)[39] and $K_4GeP_4S_{12}$ (3.0 eV)[21]. The photoluminescent spectra of **1** were studied in the solid state at room temperature, and its excitation and emission spectra are plotted in Fig. 3b. Compound **1** exhibits a broad photoluminescent emission band at 420 nm upon excitation at 295 nm.

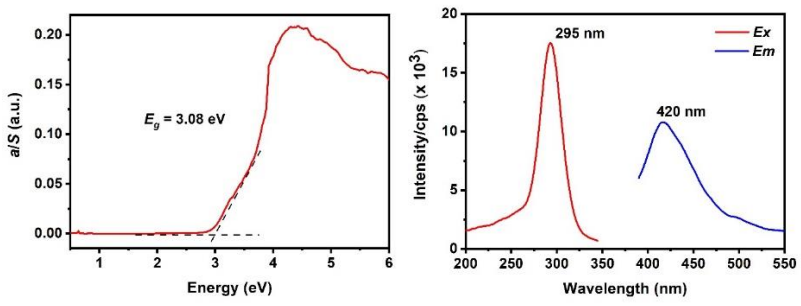

(a) (b)

Fig. 3. (a) UV-Vis diffuse reflectance spectrum and (b) excitation and emission spectra of 1

3. 3 Differential thermal analysis

The differential scanning calorimetry (DSC) was used to examine the thermal properties of **1** (Fig. 4), which showed that the compound exhibits a broad endothermic peak on the heating curve, that is, crystals of **1** melt at 645 ℃. Correspondingly, there is an exothermic peak at 626 ℃ for crystallization during the cooling process.

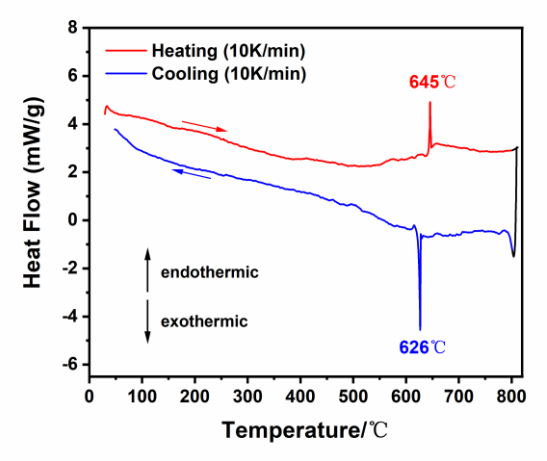

Fig. 4. DSC curves of 1

3. 4 Electronic structure calculation

To better understand the optical properties, theoretical calculations including electronic band structures and partial density of states (PDOS) of **1** are calculated by DFT. The calculated electronic band structure is plotted in Fig. 5a, indicating a direct band gap of 1.839 eV. The PDOS (Fig. 5b) shows that the conductive band (CB) close to the Fermi level is mostly composed of S-3*p* and P-3*p* states, as well as a small portion of P-3*s* state. While the valence band (VB) from –4.0 eV to the Fermi level originates predominately from S-3*p* and Ga-4*p* states. The contributions of Cs atom states to bands from –6 to 9 eV are negligible, so luminescent properties of **1** can be mainly ascribed to electron transfer from S-3*p* and Ga-4*p* states to the S-3*p* and P-3*p* ones.

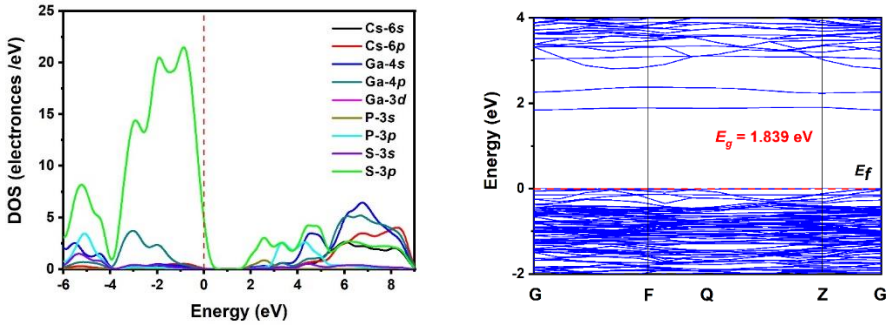

(a) (b)

Fig. 5. Electronic band structure (a) and the partial density of states (b) of 1

4 CONCLUSION

In summary, a new phase, $Cs_2Ga_3PS_8$, in triclinic space group of $P\bar{1}$ has been successfully synthesized by high-temperature reactant flux method. Its structure is built from 2*D* infinite $^2_\infty$ $[Ga_3PS_8]^{2-}$ layers, separated by Cs^+. UV-vis-NIR spectroscopy measurement indicated that $Cs_2Ga_3PS_8$ shows a wide band gap of 3.08 eV. The melting point of this compound is 645 ℃. $Cs_2Ga_3PS_8$ exhibits a broad photoluminescent emission band at 420 nm upon excitation at 295 nm. Theoretical calculation of electronic band structure indicated that fluorescent properties of $Cs_2Ga_3PS_8$ origin charge transfer from S-3*p* and Ga-4*p* states to S-3*p* and P-3*p* states.

REFERENCES

(1) Liu, B. W.; Jiang, X. M.; Zeng, H. Y.; Guo, G. C. $[ABa_2Cl][Ga_4S_8]$ (A = Rb, Cs): wide-spectrum nonlinear optical materials obtained by polycation-substitution-induced nonlinear optical (NLO)-functional motif ordering. *J. Am. Chem. Soc.* **2020**, 142, 10641−10645.

(2) Deckoff-Jones, S.; Wang, Y. X.; Lin, H. T.; Wu, W. Z.; Hu, J. J. Tellurene: a multifunctional material for midinfrared optoelectronics. *ACS Photonics* **2019**, 6, 1632−1638.

(3) Jia, H. H.; Sun, Y. L.; Zhang, Z. R.; Peng, L. F.; An, T.; Xie, J. Group 14 element based sodium chalcogenide $Na_4Sn_{0.67}Si_{0.33}S_4$ as structure template for exploring sodium superionic conductors. *Energy Storage Mater.* **2019**, 23, 508−513.

(4) Tan, C.; Cao, X.; Wu, X. J.; He, Q.; Yang, J.; Zhang, X.; Chen, J.; Zhao, W.; Han, S.; Nam, G. H.; Sindoro, M.; Zhang, H. Recent advances in ultrathin two-dimensional nanomaterials. *Chem. Rev.* **2017**, 117, 6225−6331.

(5) Liu, B. W.; Jiang, X. M.; Li, B. X.; Zeng, H. Y.; Guo, G. C. $Li[LiCs_2Cl][Ga_3S_6]$: a nanoporous framework of GaS_4 tetrahedra with excellent nonlinear optical performance. *Angew. Chem.-Int. Edit.* **2019**, 59, 4856−4859.

(6) Ye, R.; Liu, B. W.; Jiang, X. M.; Lu, J.; Zeng, H. Y.; Guo, G. C. $AMnAs_3S_6$ (A = Cs, Rb): phase-matchable infrared nonlinear optical functional motif $[As_3S_6]^{(3-)}$ obtained via surfactant-thermal method. *ACS Appl. Mater. Interfaces* **2020**, 12, 53950−53956.

(7) Yang, L. Q.; Ye, R.; Jiang, X. M.; Liu, B. W.; Zeng, H. Y.; Guo, G. C. $Ba_{13}In_{12}Zn_7S_{38}$ and $Ba_{12}In_{12}Zn_8Se_{38}$: infrared nonlinear optical chalcogenides designed by zinc-induced non-centrosymmetry transformation. *J. Mater. Chem. C* **2020**, 8, 3688−3693.

(8) Liu, B. W.; Zeng, H. Y.; Jiang, X. M.; Guo, G. C. Phase matching achieved by bandgap widening in infrared nonlinear optical materials $[ABa_3Cl_2][Ga_5S_{10}]$ (A = K, Rb, and Cs). *CCS Chem.* **2020**, 2, 964−973.

(9) Wu, K.; Yang, Y.; Gao, L. A review on phase transition and structure-performance relationship of second-order nonlinear optical polymorphs. *Coord. Chem. Rev.* **2020**, 418.

(10) Li, Z.; Zhang, S.; Huang, Z.; Zhao, L. D.; Uykur, E.; Xing, W.; Lin, Z.; Yao, J.; Wu, Y. Molecular construction from $AgGaS_2$ to $CuZnPS_4$: defect-induced second harmonic generation enhancement and cosubstitution-driven band gap enlargement. *Chem. Mater.* **2020**, 32, 3288−3296.

(11) Kutahyali Aslani, C.; Breton, L. S.; Klepov, V. V.; Zur Loye, H. C. A series of $Rb_4Ln_2(P_2S_6)(PS_4)_2$ (Ln = La, Ce, Pr, Nd, Sm, Gd) rare earth thiophosphates with two distinct thiophosphate units PVS_4^{3-} and $PIV_2S_6^4$. *Dalton Trans.* **2021**, 50, 1683−1689.

(12) Rao, R. P.; Chen, H. M.; Adams, S. Stable lithium ion conducting thiophosphate solid electrolytes $Li_{-x}(PS_4)_yX_{-z}$ (X = Cl, Br, I). *Chem. Mater.* **2019**, 31, 8649−8662.

(13) Oh, D. Y.; Ha, A. R.; Lee, J. E.; Jung, S. H.; Jeong, G.; Cho, W.; Kim, K. S.; Jung, Y. S. Wet-chemical tuning of $Li_{3-x}PS_4$ ($0 \leqslant x \leqslant 0.3$) enabled by dual solvents for all-solid-state lithium-ion batteries. *ChemSusChem.* **2020**, 13, 146−151.

(14) Schlem, R.; Till, P.; Weiss, M.; Krauskopf, T.; Culver, S. P.; Zeier, W. G. Ionic conductivity of the NASICON-related thiophosphate $Na_{1+x}Ti_{2-x}Ga_x(PS_4)_3$. *Chem. Eur. J.* **2019**, 25, 4143−4148.

(15) Zhu, Z. Y.; Chu, I. H.; Ong, S. P. $Li_3Y(PS_4)_2$ and $Li_5PS_4Cl_2$: new lithium superionic conductors predicted from silver thiophosphates using efficiently tiered *ab initio* molecular dynamics simulations. *Chem. Mater.* **2017**, 29, 2474−2484.

(16) Francisco, R. H. P.; Tepe, T.; Eckert, H. A study of the system Li–P–Se. *J. Solid State Chem.* **1993**, 107, 452−459.

(17) Chondroudis, K.; McCarthy, T. J.; Kanatzidis, M. G. Chemistry in molten alkali metal polyselenophosphate fluxes. Influence of flux composition on dimensionality. Layers and chains in $APbPSe_4$, $A_4Pb(PSe_4)_2$ (A = Rb, Cs), and $K_4Eu(PSe_4)_2$. *Inorg. Chem.* **1996**, 35, 840−844.

(18) Chung, I.; Malliakas, C. D.; Jang, J. I.; Canlas, C. G.; Weliky, D. P.; Kanatzidis, M. G. Helical polymer (1)/(infinity) $P_2Se_6^{2-}$: strong second harmonic generation response and phase-change properties of its K and Rb salts. *J. Am. Chem. Soc.* **2007**, 129, 14996−15006.

(19) Banerjee, S.; Malliakas, C. D.; Jang, J. I.; Ketterson, J. B.; Kanatzidis, M. G. 1/(infinity) $ZrPSe^{6-}$: a soluble photoluminescent inorganic polymer and

strong second harmonic generation response of its alkali salts. *J. Am. Chem. Soc.* **2008**, 130, 12270−12272.

(20) Chondroudis, K.; Kanatzidis, M. G. (1) (infinity) $P_3Se_4^-$: a novel polyanion in $K_3RuP_5Se_{10}$; formation of Ru−P bonds in a molten polyselenophosphate flux. *Angew. Chem. Int. Edit.* **1997**, 36, 1324−1326.

(21) Morris, C. D.; Chung, I.; Park, S.; Harrison, C. M.; Clark, D. J.; Jang, J. I.; Kanatzidis, M. G. Molecular germanium selenophosphate salts: phase-change properties and strong second harmonic generation. *J. Am. Chem. Soc.* **2012**, 134, 20733−20744.

(22) Banerjee, S.; Szarko, J. M.; Yuhas, B. D.; Malliakas, C. D.; Chen, L. X.; Kanatzidis, M. G. Room temperature light emission from the low-dimensional semiconductors $AZrPS_6$ (A = K, Rb, Cs). *J. Am. Chem. Soc.* **2010**, 132, 5348−5350.

(23) Chung, I.; Biswas, K.; Song, J. H.; Androulakis, J.; Chondroudis, K.; Paraskevopoulos, K. M.; Freeman, A. J.; Kanatzidis, M. G. $Rb_4Sn_5P_4Se_{20}$: a semimetallic selenophosphate. *Angew. Chem. Int. Edit.* **2011**, 50, 8834−8838.

(24) Bron, P.; Johansson, S.; Zick, K.; auf der Gunne, J. S.; Dehnen, S.; Roling, B. $Li_{10}SnP_2S_{12}$: an affordable lithium superionic conductor. *J. Am. Chem. Soc.* **2013**, 135, 15694−15697.

(25) Rigaku Oxford Diffraction. *CrysAlisPro Software System*, *Version v40.67a*, Rigaku Corporation, Oxford, UK **2019**.

(26) Siemens, *SHELXTL Version 5 Reference Manual*. Siemens Energy &Automation Inc. Madison, WI **1994**.

(27) Korum, G. *Reflectance Spectroscopy*. Springer, New York **1969**.

(28) Milman, V.; Winkler, B.; White, J. A.; Pickard, C. J.; Payne, M. C.; Akhmatskaya, E. V.; Nobes, R. H. Electronic structure, properties, and phase stability of inorganic crystals: a pseudopotential plane-wave study. *Int. J. Quantum Chem.* **2000**, 77, 895−910.

(29) Segall, M. D.; Lindan, P. J. D.; Probert, M. J.; Pickard, C. J.; Hasnip, P. J.; Clark, S. J.; Payne, M. C. First-principles simulation: ideas, illustrations and the CASTEP code. *J. Phys.*: *Condens. Matter*. **2002**, 14, 2717−2744.

(30) Morris, C. D.; Li, H.; Jin, H.; Malliakas, C. D.; Peters, J. A.; Trikalitis, P. N.; Freeman, A. J.; Wessels, B. W.; Kanatzidis, M. G. $Cs_2MIIMIV_3Q_8$ (Q = S, Se, Te): an extensive family of layered semiconductors with diverse band gaps. *Chem. Mater.* **2013**, 25, 3344−3356.

(31) Hwang, S. J.; Iyer, R. G.; Kanatzidis, M. G. Quaternary selenostannates $Na_{2-x}Ga_{2-x}Sn_{1+x}Se_6$ and $AGaSnSe_4$ (A = K, Rb, and Cs) through rapid cooling of melts. Kinetics versus thermodynamics in the polymorphism of $AGaSnSe_4$. *J. Solid State Chem.* **2004**, 177, 3640−3649.

(32) Wu, P.; Lu, Y. J.; Ibers, J. A. Synthesis and structures of the quaternary sulfides $KGaSnS_4$, $KInGeS_4$, and $KGaGeS_4$. *J. Solid State Chem.* **1992**, 97, 383−390.

(33) Jang, J. I.; Park, S.; Harrison, C. M.; Clark, D. J.; Morris, C. D.; Chung, I.; Kanatzidis, M. G. $K_4GeP_4Se_{12}$: a case for phase-change nonlinear optical chalcogenide. *Opt. Lett.* **2013**, 38, 1316−1318.

(34) Hu, X. N.; Xiong, L.; Wu, L. M. Six new members of the $A_2M(II)M(IV)_3Q_8$ family and their structural relationship. *Cryst. Growth Des.* **2018**, 18, 3124−3131.

(35) Luo, X. Y.; Liang, F.; Zhou, M. L.; Guo, Y. W.; Li, Z.; Lin, Z. S.; Yao, J. Y.; Wu, Y. C. $K_2ZnGe_3S_8$: a congruent-melting infrared nonlinear-optical material with a large band gap. *Inorg. Chem.* **2018**, 57, 9446−9452.

(36) Li, P.; Li, L. H.; Chen, L.; Wu, L. M. Synthesis, structure and theoretical studies of a new ternary non-centrosymmetric beta-$LaGaS_3$. *J. Solid State Chem.* **2010**, 183, 444−450.

(37) Luo, Z. Z.; Lin, C. S.; Cui, H. H.; Zhang, W. L.; Zhang, H.; He, Z. Z.; Cheng, W. D. SHG materials $SnGa_4Q_7$ (Q = S, Se) appearing with large conversion efficiencies, high damage thresholds, and wide transparencies in the mid-infrared region. *Chem. Mater.* **2014**, 26, 2743−2749.

(38) Lin, H.; Li, L. H.; Chen, L. Diverse closed cavities in condensed rare earth metal-chalcogenide matrixes: $CsLu_7Q_{11}$ and ($ClCs_6$) $RE_{21}Q_{34}$ (RE = Dy, Ho; Q = S, Se, Te). *Inorg. Chem.* **2012**, 51, 4588−4596.

(39) Wu, Y.; Bensch, W. Syntheses, crystal structures and spectroscopic properties of $Ag_2Nb[P_2S_6][S_2]$ and $KAg_2[PS_4]$. *J. Solid State Chem.* **2009**, 182, 471−478.